

# Competition of Dzyaloshinskii-Moriya and higher-order exchange interactions in Rh/Fe atomic bilayers on Ir(111)

Niklas Romming,<sup>1</sup> Henning Pralow,<sup>2</sup> André Kubetzka,<sup>1</sup> Markus Hoffmann,<sup>2,3</sup> Stephan von Malottki,<sup>2</sup> Sebastian Meyer,<sup>2</sup> Bertrand Dupé,<sup>4</sup> Roland Wiesendanger,<sup>1</sup> Kirsten von Bergmann,<sup>1,\*</sup> and Stefan Heinze<sup>2</sup>

<sup>1</sup>*Department of Physics, University of Hamburg, 20355 Hamburg, Germany*

<sup>2</sup>*Institut für Theoretische und Astrophysik, Christian-Albrechts-Universität zu Kiel, 24098 Kiel, Germany*

<sup>3</sup>*Peter Grünberg Institut and Institute for Advanced Simulation, Forschungszentrum Jülich and JARA, Germany*

<sup>4</sup>*Johannes Gutenberg-Universität Mainz, Institute of Physics, Staudingerweg 7, D-55128 Mainz, Germany*

(Dated: August 2, 2021)

Using spin-polarized scanning tunneling microscopy and density functional theory we demonstrate the occurrence of a novel type of noncollinear spin structure in Rh/Fe atomic bilayers on Ir(111). We find that higher-order exchange interactions depend sensitively on the stacking sequence. For fcc-Rh/Fe/Ir(111) frustrated exchange interactions are dominant and lead to the formation of a spin spiral ground state with a period of about 1.5 nm. For hcp-Rh/Fe/Ir(111) higher-order exchange interactions favor a double-row wise antiferromagnetic or  $\uparrow\uparrow\downarrow\downarrow$  state. However, the Dzyaloshinskii-Moriya interaction at the Fe/Ir interface leads to a small angle of about  $4^\circ$  between adjacent magnetic moments resulting in a canted  $\uparrow\uparrow\downarrow\downarrow$  ground state.

In systems with broken inversion symmetry and strong spin-orbit coupling the Dzyaloshinskii-Moriya interaction (DMI) [1, 2] plays an essential role for the formation of topologically non-trivial spin structures such as skyrmions [3–11]. At transition-metal surfaces and interfaces the DM interaction can induce numerous types of non-collinear spin structures such as cycloidal spin spirals [12–14], Néel type domain walls [15–20], as well as skyrmions and skyrmion lattices [21–29].

In such systems there is a competition between the DMI favoring a non-collinear spin structure and the Heisenberg exchange, which typically favors collinear alignment of magnetic moments. Depending on their strength and the magnetocrystalline anisotropy energy a spin spiral state forms in zero magnetic field and a transition to skyrmions occurs at finite field. However, higher-order exchange interactions such as the four-spin or bi-quadratic term can lead to more complex spin structures e.g. multi-Q states [30], conical spin spirals [31] or atomic-scale skyrmion lattices [21, 26]. For an Fe monolayer on the Rh(111) surface a so-called up-up-down-down ( $\uparrow\uparrow\downarrow\downarrow$ ) or double-row wise antiferromagnetic state has been predicted [32, 33] based on density functional theory (DFT), however, not observed experimentally yet.

Here, we demonstrate that the interplay of the DMI and higher-order exchange can lead to the formation of a novel type of canted  $\uparrow\uparrow\downarrow\downarrow$ -state, with small angles between adjacent magnetic moments. We study atomic Rh/Fe bilayers on the Ir(111) surface which grow pseudomorphically as shown by scanning tunneling microscopy (STM) measurements. While Fe grows in fcc stacking both hcp and fcc stacking of Rh are observed. The ground state spin structure of the film depends on the stacking of the Rh overlayer. In the fcc stacking we observe a spin spiral state in spin-polarized (SP-) STM images with a period of 1.5 nm, which is driven by the frustration of exchange interactions as shown from DFT

calculations. However, for the hcp stacking of Rh an  $\uparrow\uparrow\downarrow\downarrow$ -state is favorable due to higher-order exchange interactions. SP-STM shows a stripe pattern with a periodicity close to the four atomic rows spin structure realized in the  $\uparrow\uparrow\downarrow\downarrow$ -state. Using non-spin-polarized STM we find a strong electronic contrast which is explained by the inhomogeneous spin polarization of the Rh overlayer. Spin-polarized STM with different tip magnetization directions demonstrates that the spin structure is non-collinear suggesting a small canting of the magnetic moments relative to the collinear  $\uparrow\uparrow\downarrow\downarrow$ -state. We show that this canted spin state is driven by the DMI which is significant at the Fe/Ir interface.

An STM measurement of a typical Rh/Fe/Ir(111) sample is shown in Fig. 1(a), where the color coding refers to the local differential conductance ( $dI/dU$ ) (see [34] for the sample preparation). At this bias voltage, Fe and Ir have similar  $dI/dU$  signals, but there are two clearly distinguishable contrast levels for the Rh islands. The signal strength correlates with the orientation of the roughly triangular Rh islands, a sign of pseudomorphic growth of Rh with both possible stackings exhibiting slightly different electronic properties. We assign the darker  $dI/dU$  signal at this bias voltage to fcc-Rh and the brighter one to hcp-Rh (see [34] for experimental details).

In order to investigate the structural, electronic and magnetic properties of such atomic Rh/Fe bilayers on the Ir(111) surface we have performed DFT calculations using the FLEUR code (see [34] for computational details). We start by discussing the energy dispersion  $E(\mathbf{q})$  of flat homogeneous spin spirals obtained without taking spin-orbit coupling (SOC) into account, black data in Fig. 1(b). The energy dispersions show that the ferromagnetic (FM) state at  $\bar{\Gamma}$  has lower energy than the antiferromagnetic (AFM) state at the Brillouin zone boundary. For both Rh stackings there are deep energy minima on the order of 10–15 meV/Fe atom for spin spirals with

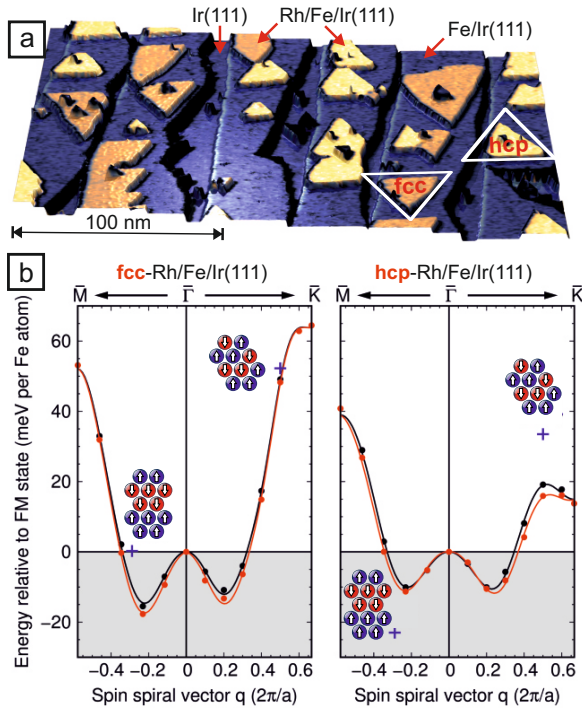


FIG. 1. (a) Perspective STM constant-current image of a typical Rh/Fe/Ir(111) sample with approx. 0.8 ML Fe and 0.4 ML Rh, colored with the simultaneously acquired  $dI/dU$  signal ( $U = +0.5$  V,  $I = 0.75$  nA,  $T = 8$  K). (b) Calculated energy dispersions  $E(\mathbf{q})$  of right-rotating cycloidal homogeneous spin spirals for fcc-Rh (left) and hcp-Rh (right) on Fe/Ir(111) without spin-orbit coupling (black symbols) and with spin-orbit coupling (red symbols). The lines denote fits to the Heisenberg model including the Dzyaloshinskii-Moriya interaction for the case with spin-orbit coupling (see [34] for details). The energies of the  $\uparrow\uparrow\downarrow\downarrow$ -states along the two high symmetry directions are marked by blue crosses and the spin structures are sketched as insets.

periods of  $\lambda \approx 1.2$  nm. The origin of these spin spiral minima is frustration of exchange interactions, where the nearest-neighbor exchange interaction favors FM alignment, but 2nd or 3rd nearest neighbor exchange interactions are AFM (for exchange constants see [34]).

Including spin-orbit coupling (SOC), see red data in Fig. 1(b), leads to a preference of right rotating cycloidal spin spirals due to DMI for both types of stacking of the Rh overlayer. However, the energy differences are relatively small compared to the depths of the spin spiral energy minima neglecting SOC.

Because a significant role of higher-order exchange interactions has been reported for the Fe/Rh [32, 33] and Fe/Ir [21] interfaces, we have also considered collinear  $\uparrow\uparrow\downarrow\downarrow$ -states along the high symmetry directions. These states are formed by the superposition of spin spirals and should be energetically degenerate with them within the Heisenberg model. Energy differences obtained within DFT indicate higher-order exchange contributions. For

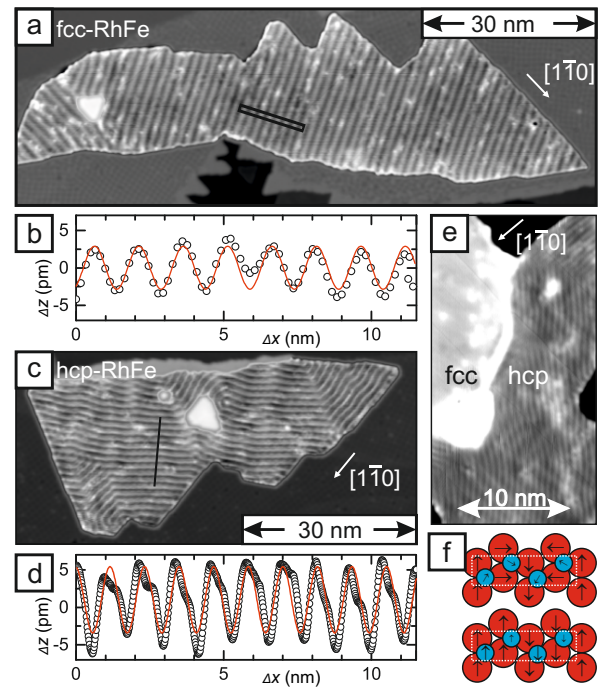


FIG. 2. (a),(c) SP-STM constant-current images of an fcc-Rh and an hcp-Rh island on Fe/Ir(111), respectively, measured with a magnetic Cr tip, sensitive to the out-of-plane magnetization component of the sample (contrast level adjusted locally on the Rh/Fe to  $\pm 20$  pm;  $T = 8$  K,  $U = +30$  and  $-30$  mV,  $I = 1.0$  and  $1.5$  nA, respectively). (b),(d) Line profiles along the rectangles in (a,c); solid lines are fits with cosine-functions. (e) Constant-current STM image of a Rh island with fcc and hcp stacking on fcc-Fe/Ir(111) measured with a non-spin-polarized tip (contrast  $\pm 15$  pm;  $T = 8$  K,  $U = +15$  mV,  $I = 6$  nA). (f) Top-view sketches of a homogeneous 4 atom period spin spiral and the  $\uparrow\uparrow\downarrow\downarrow$ -state; Fe atoms in red and Rh atoms in blue, the magnetic unit cell is indicated by the dotted box; for simplicity in-plane magnetic states are sketched.

fcc-Rh we find that both  $\uparrow\uparrow\downarrow\downarrow$ -states have a higher energy compared to the respective spin spirals, and the magnetic ground state remains a spin spiral along  $\overline{\Gamma M}$  [Fig. 1(b)]. For hcp-Rh we find that the  $\uparrow\uparrow\downarrow\downarrow$ -state along the  $\overline{\Gamma K}$  direction is about 34 meV/Fe-atom higher than the FM state, however, the  $\uparrow\uparrow\downarrow\downarrow$ -state along the  $\overline{\Gamma M}$  direction is by about 12 meV/Fe-atom lower in energy than the lowest spin spiral state [Fig. 1(b)].

When a magnetic tip is used in STM the tunnel magnetoresistance (TMR) effect occurs, which leads to a SP contribution to the tunnel current in addition to the structural and electronic part [35, 36]. Figure 2(a) shows such an SP-STM measurement of an fcc-Rh/Fe island exhibiting a cosine-like magnetic modulation with a period  $\lambda_{\text{fcc}} \approx 1.5$  nm (see Fig. 2(b)) and propagation along  $(11\bar{2})$  directions. We conclude that fcc-Rh/Fe exhibits a spin spiral ground state with a continuous rotation of adjacent magnetic moments (see [34] for further measurements),

in agreement with the spin spiral energy minimum found along the  $\bar{\Gamma}\text{M}$  direction from DFT (cf. Fig. 2(a)) [37].

The SP-STM image in Fig. 2(c) shows an hcp-Rh/Fe island and a similar stripe pattern with a slightly smaller period ( $\lambda_{\text{hcp}} \approx 1.1$  nm) is visible. The magnetic structure differs from the one in fcc-Rh/Fe islands in subtle aspects: the propagation direction seems to be more flexible, is not strictly along  $(11\bar{2})$  directions but instead varies locally; the shape of the periodic signal significantly differs from a cosine, compare profile in Fig. 2(d). This demonstrates that the magnetic ground state of the hcp-Rh/Fe island is different to that of fcc-Rh/Fe.

Because in STM several different magnetoresistive (MR) effects can contribute to the measurement signal [38, 39], in Fig. 2(e) we use a non-spin-polarized tip to separate purely electronic contributions from signal variations due to the TMR. We find that for fcc and hcp-Rh the TMR signals with periods of about 1.5 nm and 1.1 nm, respectively, vanish, meaning that they originate from TMR. On fcc-Rh on Fe/Ir(111) no remaining modulation of the signal is observed in the bias voltage regime  $\pm 1$  V. In contrast, the non-spin-polarized signal observed on hcp-Rh is rather strong, i.e. on the order of a few pm, with half of the magnetic period, see Fig. 2(e), and can be observed in a bias voltage regime of around  $\pm 0.2$  V.

Regarding the purely electronic contributions to magnetoresistance, the generic differences between a spin spiral and an  $\uparrow\uparrow\downarrow$ -state, as predicted by DFT for our atomic Rh/Fe bilayer system, can be understood based on the sketches in Fig. 2(f). The tunnel anisotropic magnetoresistance (TAMR) [38] due to spin-orbit coupling can occur for spin spirals (in-plane spins are inequivalent to out-of-plane spins) and would manifest as a modulation with half of the magnetic period, but it is absent in a collinear magnetic state as the  $\uparrow\uparrow\downarrow$ -state. Regarding the non-collinear magnetoresistance [39], the four-atom magnetic period is a special case where the contribution to the total magnetoresistance does not vary locally.

We can calculate STM images for the  $\uparrow\uparrow\downarrow$ -state of hcp-Rh/Fe/Ir(111) directly from DFT. Within the Tersoff-Hamann model [40] and its generalization to the spin-polarized case [41] the STM image corresponds to the (spin-resolved) local density of states (LDOS) a few  $\text{\AA}$  above the surface. The simulated SP-STM image [Fig. 3(a)] assuming a small negative bias voltage of 0.1 V shows a stripe pattern with the magnetic period corresponding to the  $\uparrow\uparrow\downarrow$ -state. The scan lines display an asymmetric shape as seen in Fig. 3(c). If we assume a vanishing spin-polarization of the tip in our calculations we obtain the STM image in Fig. 3(b). We find a stripe pattern with half the magnetic period as in the experiment. As shown by the scan lines given in Fig. 3(c), the corrugation amplitude amounts to a few pm.

This electronic effect has been predicted before based on DFT for the  $\uparrow\uparrow\downarrow$ -state in an Fe monolayer on Rh(111) [33]. For Rh/Fe/Ir(111) the effect is much en-

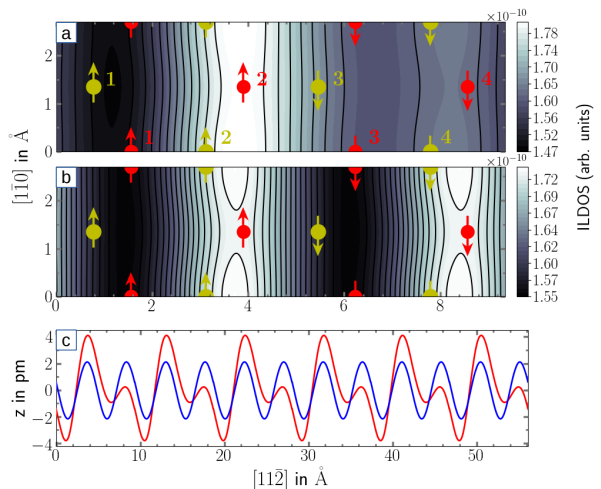


FIG. 3. STM images simulated based on the DFT calculations for the  $\uparrow\uparrow\downarrow$  state along  $\bar{\Gamma}\text{M}$  of hcp-Rh/Fe/Ir(111). (a) STM image at a tip-sample distance of  $z = 6.7$   $\text{\AA}$  and for a tip spin polarization of 0.5. The red and yellow filled circles represent the Fe and Rh atoms, respectively, and the arrows show the direction of the magnetic moments in the  $\uparrow\uparrow\downarrow$  state. Note that the moments have been drawn in the film plane for illustration although the easy axis is perpendicular to the film. (b) simulated STM image for a non-spin-polarized STM tip. (c) Line scans along the  $[11\bar{2}]$  direction for the simulated STM images in (a) (red line) and in (b) (blue line). States between the Fermi energy  $E_F$  and 0.1 eV below  $E_F$  have been taken into account for the simulated STM images.

hanced as it originates from the interface with the Rh layer which is at the surface in our case. The  $\uparrow\uparrow\downarrow$ -state can be viewed as the extreme limit of an inhomogeneous spin spiral, and the Rh atoms become inequivalent and have different magnetic moments depending on whether all three neighboring Fe atoms are parallel ( $m_{\text{Rh1}}^{\text{hcp}} = \pm 0.43\mu_B$ ) or two are antiparallel and only one is parallel ( $m_{\text{Rh2}}^{\text{hcp}} = \pm 0.08\mu_B$ ) (see sketch in Fig. 2f).

To investigate experimentally whether the hcp-Rh/Fe exhibits a strictly collinear magnetic ground state we image the out-of-plane and the in-plane magnetization components of the same island, see Fig. 4(a) and (b), respectively. This is done by using an Fe-coated W tip that aligns its magnetization in out-of-plane magnetic fields and thus detects out-of-plane sample magnetization components, whereas it has a magnetization in the surface plane without external magnetic field, thus being sensitive to the in-plane magnetization components of the sample. Figure 4(a) demonstrates that in measurements with an out-of-plane sensitive tip all three rotational domains appear the same; the pattern consists of slim bright lines spaced with the magnetic periodicity. Such a pattern is observed when the magnetic and the electronic MR contributions are of similar magnitude and in phase, i.e. the magnetic maxima/minima coincide with the maxima of the electronic contribution and thus

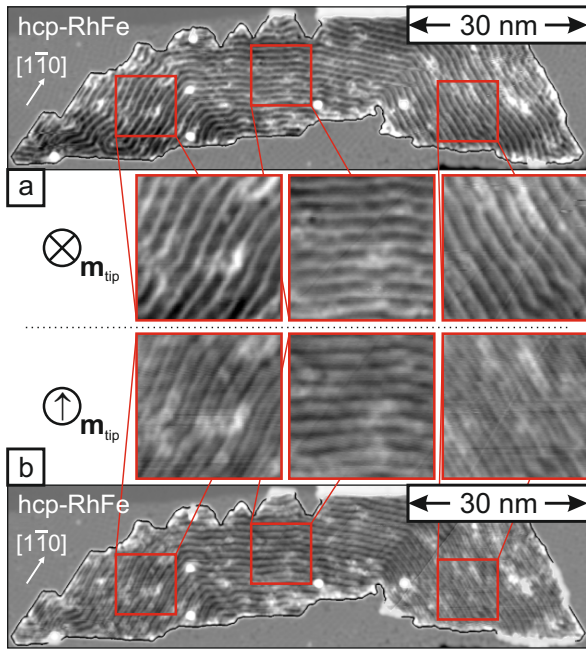


FIG. 4. (a),(b) Constant-current SP-STM images of a hcp-Rh island on Fe/Ir(111) measured with out-of-plane sensitive and in-plane sensitive magnetic Fe-coated W tip, respectively; the tip magnetization  $\mathbf{m}_{tip}$  aligns in the applied out-of-plane field of  $B = -2$  T (a), but is in the sample surface plane without applied field (b); its direction as indicated is derived from comparison of the relative magnetic contrast amplitudes of the three symmetry-equivalent rotational domains, see enlarged images (all contrast levels adjusted locally to  $\pm 15$  pm) ( $T = 8$  K,  $U = +30$  mV,  $I = 3$  nA).

add-up/cancel [42].

The SP-STM image with in-plane magnetized tip in Fig. 4(b) shows a qualitatively different pattern in the central rotational domain compared to the two other rotational domains. This immediately means that there are also magnetic in-plane components in the sample; given that the spin texture is of cycloidal nature due to the DMI, we can derive a tip magnetization axis as indicated, leading to a large magnetic contribution to the signal for the central domain. The magnetic signal is small in the other two domains and there the electronic contribution with half the magnetic period dominates the image. From these measurements we conclude that we have both out-of-plane as well as in-plane magnetization components in this sample and can thus rule out a strictly collinear  $\uparrow\uparrow\downarrow$  state. However, because of the large electronic effect observed experimentally, which we attribute to the polarization variation of the Rh atoms, we propose that the hcp-Rh/Fe/Ir(111) realizes a magnetic state in between the two extreme cases of homogeneous spin spiral and  $\uparrow\uparrow\downarrow$  (see Fig. 2(f)), i.e. an inhomogeneous spin spiral or a canted  $\uparrow\uparrow\downarrow$ -state. Because the periodic modulation of the LDOS as manifested in the electronic contrast also changes the spin-polarization of the Rh atoms

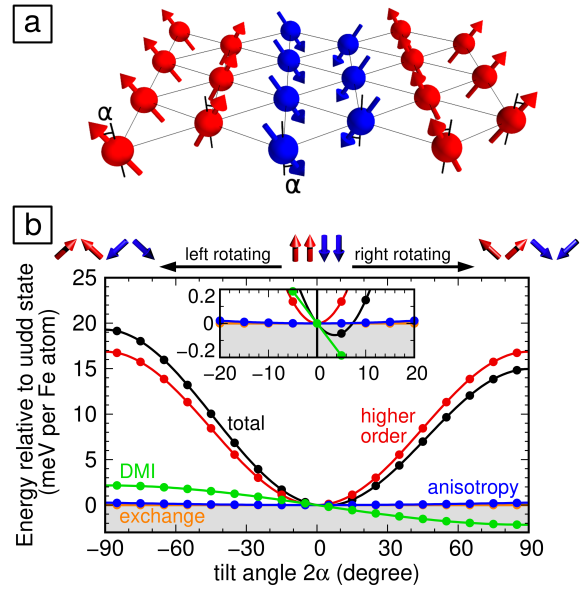


FIG. 5. (a) Sketch of the canted  $\uparrow\uparrow\downarrow$  state defined by the angle  $\alpha$ . Only the magnetic moments in the Fe layer are shown. Blue and red denotes an up- or downwards out-of-plane magnetization component. (b) Energy as a function of  $\alpha$  resolved by the contributions from different magnetic interactions. The filled circles are obtained numerically using the DFT interaction parameters for the atomistic spin model and the lines are from the analytical forms of the energy contributions (see text). Note that positive/negative values of  $\alpha$  indicate an anti-clockwise/clockwise rotation of the magnetic moments.

(see Fig. S6 [34]), we cannot quantitatively compare the measured magnetic amplitudes to extract the canting angle.

The DFT calculations of Fig. 1(b) have considered homogeneous spin spirals and collinear  $\uparrow\uparrow\downarrow$ -states. To include inhomogeneous spin spirals, as found experimentally, and study which energy contributions could lead to such a state, we introduce a canting angle  $\alpha$  relative to the easy magnetization axis, see Fig. 5(a). This allows to continuously transform the  $\uparrow\uparrow\downarrow$ -state ( $\alpha = 0^\circ$ ) to the  $90^\circ$  clockwise spin spiral ( $\alpha = 45^\circ$ ). Negative values of  $\alpha$  denote an anti-clockwise spin canting. It can easily be shown that the exchange energy contribution does not depend on  $\alpha$ . The magnetocrystalline anisotropy energy stabilizes the collinear state and varies as  $E_{MAE} \propto -\cos^2 \alpha$ , however, the MAE is small with  $0.53$  meV/Fe-atom. The DMI favors a canting and decreases as  $E_{DMI} \propto -\sin 2\alpha$  for clockwise spin canting (Fig. 5(b)). Note that the strength of the DMI and the MAE are obtained from DFT. The energy difference of about  $17$  meV/Fe-atom between the  $\uparrow\uparrow\downarrow$  and the  $90^\circ$  spin spiral state can only be due to higher-order exchange contributions since spin-orbit coupling has been turned off in the DFT calculation. This leads to a rise with  $(1 - \cos^2 \alpha)$  if we assume only nearest-neighbor four-spin

and biquadratic interaction (see Eqs. (3) and (4) in [34]). The competition of DMI and these higher-order contributions leads to an energy minimum at a canting angle of  $2\alpha \approx 4^\circ$  between adjacent spins which are parallel in the collinear  $\uparrow\uparrow\downarrow\downarrow$ -state.

To check the validity of the spin model we have performed self-consistent non-collinear DFT calculations including spin-orbit coupling in the four atom per layer super cell of the  $\uparrow\uparrow\downarrow\downarrow$  state allowing the spins to relax to find the energetically most favorable state [43]. To make these calculations computationally feasible, we have considered a freestanding Rh/Fe/Ir trilayer which is very similar to the Rh/Fe/Ir(111) film system in terms of its magnetic properties (see [34] for details). We find a canted  $\uparrow\uparrow\downarrow\downarrow$  state with  $2\alpha \approx 7^\circ$  energetically more favorable by 0.03 meV/Fe-atom than the collinear  $\uparrow\uparrow\downarrow\downarrow$ -state. Two of the Rh magnetic moments point almost perpendicular to the surface while the other two are at angles of about  $13^\circ$  with respect to the surface normal (see Fig. S4 [34]). Thus the in-plane components are enhanced at the Rh surface layer which explains the relatively strong in-plane contrast observed in SP-STM measurements (cf. Fig. S7 [34]).

In conclusion, we have shown that higher-order exchange interactions can play a decisive role in transition-metal trilayers and may compete with interfacial DM interactions. Our work demonstrates that higher-order exchange needs to be taken into account in the search for novel transition-metal interfaces potentially promising for complex non-collinear spin structures such as skyrmions.

This work has received financial support by the European Union via the Horizon 2020 research and innovation programme under grant agreement No. 665095 (FET-Open project MagicSky), and by the Deutsche Forschungsgemeinschaft via SFB668-A8. We gratefully acknowledge computing time at the supercomputer of the North-German Supercomputing Alliance (HLRN).

---

\* Email: kbergman@physnet.uni-hamburg.de

- [1] I. E. Dzyaloshinskii, *Sov. Phys. JETP* **5**, 1259 (1957).
- [2] T. Moriya, *Phys. Rev.* **120**, 91 (1960).
- [3] A. Bogdanov and D. A. Yablonskii, *Sov. Phys. JETP* **68**, 101 (1989).
- [4] A. Bogdanov and A. Hubert, *J. Mag. Mag. Mat.* **138**, 255 (1994).
- [5] A. N. Bogdanov and U. K. Rößler, *Phys. Rev. Lett.* **87**, 037203 (2001).
- [6] S. Mühlbauer, B. Binz, F. Jonietz, C. Pfleiderer, A. Rosch, A. Neubauer, R. Georgii, and P. Böni, *Science* **323**, 915 (2009).
- [7] X. Z. Yu, Y. Onose, N. Kanazawa, J. H. Park, J. H. Han, Y. Matsui, N. Nagaosa, and Y. Tokura, *Nature* **465**, 901 (2010).
- [8] S. Seki, X. Z. Yu, S. Ishiwata, and Y. Tokura, *Science* **336**, 198 (2012).
- [9] A. Fert, V. Cros, and J. Sampaio, *Nat. Nanotechnol.* **8**, 152 (2013).
- [10] N. Nagaosa and Y. Tokura, *Nat. Nanotechnol.* **8**, 899 (2013).
- [11] R. Wiesendanger, *Nat. Rev. Mat.* **1**, 16044 (2016).
- [12] M. Bode, M. Heide, K. von Bergmann, P. Ferriani, S. Heinze, G. Bihlmayer, a. Kubetzka, O. Pietzsch, S. Blügel, and R. Wiesendanger, *Nature* **447**, 190 (2007).
- [13] P. Ferriani, K. von Bergmann, E. Y. Vedmedenko, S. Heinze, M. Bode, M. Heide, G. Bihlmayer, S. Bluegel, and R. Wiesendanger, *Phys. Rev. Lett.* **101**, 027201 (2008).
- [14] S. H. Phark, J. A. Fischer, M. Corbetta, D. Sander, K. Nakamura, and J. Kirschner, *Nat. Commun.* **5**, 5183 (2014).
- [15] A. Kubetzka, O. Pietzsch, M. Bode, and R. Wiesendanger, *Phys. Rev. B* **67**, 020401 (2003).
- [16] M. Heide, G. Bihlmayer, and S. Blügel, *Phys. Rev. B* **78**, 140403 (2008).
- [17] S. Meckler, N. Mikuszeit, A. Pressler, E. Y. Vedmedenko, O. Pietzsch, and R. Wiesendanger, *Phys. Rev. Lett.* **103**, 157201 (2009).
- [18] G. Chen, J. Zhu, A. Quesada, J. Li, A. T. N'Diaye, Y. Huo, T. P. Ma, Y. Chen, H. Y. Kwon, C. Won, et al., *Phys. Rev. Lett.* **110**, 177204 (2013).
- [19] S. Emori, U. Bauer, S. Ahn, E. Martinez, and G. Beach, *Nat. Mater.* **12**, 611 (2013).
- [20] K. Ryu, L. Thomas, S. Yang, and S. Parkin, *Nat. Nanotechnol.* **8**, 527 (2013).
- [21] S. Heinze, K. von Bergmann, M. Menzel, J. Brede, A. Kubetzka, R. Wiesendanger, G. Bihlmayer, and S. Blügel, *Nat. Phys.* **7**, 713 (2011).
- [22] N. Romming, C. Hanneken, M. Menzel, J. E. Bickel, B. Wolter, K. von Bergmann, A. Kubetzka, and R. Wiesendanger, *Science* **341**, 636 (2013).
- [23] N. Romming, A. Kubetzka, C. Hanneken, K. von Bergmann, and R. Wiesendanger, *Phys. Rev. Lett.* **114**, 177203 (2015).
- [24] G. Chen, A. Mascaraque, A. T. N'Diaye, and A. K. Schmid, *Appl. Phys. Lett.* **106**, 242404 (2015).
- [25] W. Jiang, P. Upadhyaya, W. Zhang, G. Yu, M. B. Jungfleisch, F. Y. Fradin, J. E. Pearson, Y. Tserkovnyak, K. L. Wang, O. Heinonen, et al., *Science* **349**, 283 (2015).
- [26] M. Hoffmann, J. Weischenberg, B. Dupé, F. Freimuth, P. Ferriani, Y. Mokrousov, and S. Heinze, *Phys. Rev. B* **92**, 020401(R) (2015).
- [27] O. Boule, J. Vogel, H. Yang, S. Pizzini, D. de Souza Chaves, A. Locatelli, T. O. Mente, A. Sala, L. D. Buda-Prejbeanu, O. Klein, et al., *Nat. Nanotechnol.* **11**, 449 (2016).
- [28] C. Moreau-Lucaire, C. Moutafis, N. Reyren, J. Sampaio, C. A. F. Vaz, N. Van Horne, K. Bouzehouane, K. Garcia, C. Deranlot, P. Warnicke, et al., *Nat. Nanotechnol.* **11**, 444 (2016).
- [29] S. Woo, K. Litzius, B. Krüger, M.-Y. Im, L. Caretta, K. Richter, M. Mann, A. Krone, R. M. Reeve, M. Weigand, et al., *Nat. Mater.* **15**, 501 (2016).
- [30] P. Kurz, G. Bihlmayer, K. Hirai, and S. Blügel, *Phys. Rev. Lett.* **86**, 1106 (2001).
- [31] Y. Yoshida, S. Schröder, P. Ferriani, D. Serrate, A. Kubetzka, K. von Bergmann, S. Heinze, and R. Wiesendanger, *Phys. Rev. Lett.* **108**, 087205 (2012).
- [32] B. Hardrat, A. Al-Zubi, P. Ferriani, S. Blügel,

- G. Bihlmayer, and S. Heinze, Phys. Rev. B **79**, 094411 (2009).
- [33] A. Al-Zubi, G. Bihlmayer, and S. Blügel, Phys. Status Solidi B **248**, 2242 (2011).
- [34] Supplemental material.
- [35] M. Bode, Rep. Prog. Phys. **66**, 523 (2003).
- [36] R. Wiesendanger, Rev. Mod. Phys. **81**, 1495 (2009).
- [37] With an external magnetic field a skyrmion lattice phase can in principle be induced as shown by spin dynamics simulations (see [34]), however, due to the deep energy minimum the transition fields are about 50 T.
- [38] M. Bode, S. Heinze, A. Kubetzka, O. Pietzsch, X. Nie, G. Bihlmayer, S. Blügel, and R. Wiesendanger, Phys. Rev. Lett. **89**, 237205 (2002).
- [39] C. Hanneken, F. Otte, A. Kubetzka, B. Dupé, N. Romming, K. von Bergmann, R. Wiesendanger, and S. Heinze, Nature Nanotech. **10**, 1039 (2015).
- [40] J. Tersoff and D. R. Hamann, Phys. Rev. B **31**, 805 (1985).
- [41] D. Wortmann, S. Heinze, P. Kurz, G. Bihlmayer, and S. Blügel, Phys. Rev. Lett. **86**, 4132 (2001).
- [42] K. von Bergmann, M. Menzel, D. Serrate, Y. Yoshida, S. Schröder, P. Ferriani, A. Kubetzka, R. Wiesendanger, and S. Heinze, Phys. Rev. B **86**, 134422 (2012).
- [43] P. Kurz, F. Förster, L. Nordström, G. Bihlmayer, and S. Blügel, Phys. Rev. B **69**, 024415 (2004).